NASA Contractor Report 189646
ICASE Report No. 92–19

ICASE

SYSTEMATIC STUDY OF REYNOLDS STRESS CLOSURE MODELS IN THE COMPUTATIONS OF PLANE CHANNEL FLOWS

A. O. Demuren
S. Sarkar

Contract No. NAS1–18605
April 1992

Institute for Computer Applications in Science and Engineering
NASA Langley Research Center
Hampton, Virginia 23665–5225

Operated by the Universities Space Research Association

National Aeronautics and
Space Administration

Langley Research Center
Hampton, Virginia 23665-5225

SYSTEMATIC STUDY OF REYNOLDS STRESS CLOSURE MODELS IN THE COMPUTATIONS OF PLANE CHANNEL FLOWS

*A. O. Demuren**
Department of Mechanical Engineering and Mechanics
Old Dominion University
Norfolk, VA 23529

and

S. Sarkar **
Institute for Computer Applications in Science and Engineering
NASA Langley Research Center
Hampton, VA 23665

ABSTRACT

This paper investigates the roles of pressure-strain and turbulent diffusion models in the numerical calculation of turbulent plane channel flows with second-moment closure models. Three turbulent diffusion and five pressure-strain models are utilized in the computations. The main characteristics of the mean flow and the turbulent fields are compared against experimental data. All the features of the mean flow are correctly predicted by all but one of the Reynolds stress closure models. The Reynolds stress anisotropies in the log layer are predicted to varying degrees of accuracy (good to fair) by the models. None of the models could predict correctly the extent of relaxation towards isotropy in the wake region near the center of the channel. Results from the direct numerical simulation are used to further clarify this behaviour of the models.

*This research was supported by the National Aeronautics and Space Administration under NASA Contract No. NAS1-18605 while the authors were in residence at the Institute for Computer Applications in Science and Engineering (ICASE), NASA Langley Research Center, Hampton, VA 23665.

1. Introduction

Second-moment turbulence closure models first appeared about four decades ago with the proposal of a simple linear model for the pressure-strain correlation by Rotta (1951). Models with increasing complexity and sophistication have followed. The milestones are the works of Daly and Harlow (1970) (denoted DH), Hanjalic and Launder (1972) (denoted HL), Launder, Reece and Rodi (1975) (denoted LRR), Shih and Lumley (1985) (denoted SL), Fu, Launder and Tselepidakis (1987) (denoted FLT), and Speziale, Sarkar and Gatski (1991) (denoted SSG). Speziale (1991) has presented an insightful review of this hierarchy of closure models. The earlier models (DH, HL and LRR) propose approximations for the pressure-strain correlations which are linear in the Reynolds stresses, whereas the latter models (SL, FLT and SSG) use non-linear terms for these correlations. Although second-moment closure models have a sounder theoretical basis than eddy-viscosity based models such as the k-ϵ model, their superiority in predictive ability has not been demonstrated in a consistent and systematic manner. Most of the models were derived with the use of homogeneous flow assumptions and the original applications have emphasized the prediction of homogeneous or nearly-homogeneous flows. There is a need for systematic studies in which the models are applied to flows with increasing complexity which are of practical importance, and the computed results compared to experimental data and results obtained with two-equation models, with the goal of establishing their capabilities and inadequacies. It is more usual to see a quantum leap in the application of the models to calculate highly complex two- and three-dimensional flows (Amano and Goel, 1987; Sykes et al., 1986; Demuren, 1992). From the point of view of developing turbulence models, such an exercise is usually inconclusive since the performance of the models in the (inhomogeneous) elementary or component flows is not well known.

The present study is the first stage of an attempt to bridge this gap. The pressure-strain models tested here are : the quasi-isotropic model of LRR with and without wall-reflection terms, the models of SSG, SL and FLT, all without any special wall-proximity treatment. Three formulations for the diffusion terms are also examined. These are proposals by DH, HL and MH

(Mellor and Herring, 1973). The first has been criticized for violating the symmetry of indices in $\overline{u_i u_j u_k}$ (the triple velocity correlation) but is still widely used because of its simplicity. The last two preserve this symmetry in the indices of $\overline{u_i u_j u_k}$.

The test problem is the fully-developed plane channel flow at high Reynolds number. Surprisingly, it was difficult to find complete sets of experimental data which fulfill the following requirements ; high Reynolds number, high aspect ratio, long development length and high accuracy and consistency. Comte-Bellot (1965) presented data at very high Reynolds numbers but these showed an inexplicable Reynolds number dependence. Channel flow data by Clark (1968) also showed an excessive dependence on Reynolds number, and values of the normalized turbulent kinetic energy k/U_τ^2 appeared to be too high in the near wall region. Laufer (1951) presented data for a 12:1 aspect ratio channel at Reynolds numbers (based on bulk mean velocity and half-width) in the range 10,300 to 52,000 taken at 86 half-widths from the inlet. Hussain and Reynolds (1975) suggested that this length would be insufficient for full development of the turbulence field. They presented measurements at 450 half-widths to support this, but their data set was incomplete since only the longitudinal normal stress component was given. A review of duct flow measurements by Klein (1981) supports their assertion. Nevertheless, Laufer's data represent then the best compromise, and hence was used to construct the anisotropy stress tensor components to which the present model computations are compared. It was supplemented with direct simulation results of Kim, Moin and Moser (1987) (denoted as KMM), and Kim (unpublished), in order to explore more detailed features of the turbulence fields in comparison to the turbulence models.

2. Mathematical Formulation

2.1 Mean Flow Equations

The Reynolds-averaged mean-flow equations for steady, incompressible turbulent flow can be written in Cartesian tensor notation as:

Continuity

$$\frac{\partial U_i}{\partial x_i} = 0 \tag{1}$$

Momentum

$$\frac{\partial}{\partial x_l}(U_l U_i) = -\frac{1}{\rho}\frac{\partial P}{\partial x_i} + \frac{\partial}{\partial x_l}\left[-\overline{u_i u_l} + \frac{\mu}{\rho}\left(\frac{\partial U_i}{\partial x_l} + \frac{\partial U_l}{\partial x_i}\right)\right] \tag{2}$$

where $x_i=(x_1, x_2, x_3)$ represent the Cartesian coordinates, $U_i=(U_1,U_2,U_3)$ the Cartesian mean velocity components, P is the pressure, μ the molecular viscosity and ρ the density. Einstein's summation rule for repeated indices is utilized. $\overline{u_i u_l}$ (with i=1,2,3, and l=1,2,3) represents the six components of the Reynolds stress tensor, R_{il} which must be determined by the turbulence model.

If, in the fully-developed plane channel flow, the walls are in the (1 —3) planes as shown in Fig. 1, then, $\frac{\partial}{\partial x_1} = \frac{\partial}{\partial x_3} = 0$ in equations (1) and (2). Also, the Reynolds stress tensor R_{il} will have only 4 non-zero components; the three diagonal elements $\overline{u_1^2}, \overline{u_2^2}$ and $\overline{u_3^2}$ which represent the normal stresses, and one off-diagonal element $\overline{u_1 u_2}$ which represents the shear stress.

2.2 Reynolds Stress Equations

The transport equations for the Reynolds stress components can be written for high Reynolds number turbulent flow in Cartesian tensor notation as:

$$\frac{\partial}{\partial x_l}(U_l \overline{u_i u_j}) = D_{ij} + P_{ij} + \pi_{ij} - \epsilon_{ij} \tag{3}$$

where D_{ij} is the diffusion, P_{ij} is the production, π_{ij} is the pressure-strain correlation, and ϵ_{ij} is the dissipation rate.

The production term is $P_{ij} = -\overline{u_i u_l}\frac{\partial U_j}{\partial x_l} - \overline{u_j u_l}\frac{\partial U_i}{\partial x_l}$; and the dissipation is assumed to be locally isotropic so that $\epsilon_{ij} = 2/3\,\delta_{ij}\epsilon$, where ϵ is the dissipation rate of the turbulent kinetic energy k, to be determined from the solution of a transport equation, and δ_{ij} is the Kronecker delta. However, FLT attempts to account for anisotropy in the dissipation, as will be discussed in a later section.

The models for D_{ij} and π_{ij} are the subjects of the present study.

2.3 Diffusion Models

The three diffusion models examined are based on the proposals of DH, HL, and MH. They are written in tensor form as,

$$D_{ij} = \left(-T_{ijk}\right)_{,k} \tag{4}$$

where $(\ )_{,k}$ represents the first derivative with respect to x_k, and T_{ijk} is given by:

$$\text{DH} : \quad -T_{ijk} = c_{s1}\frac{k}{\epsilon}\left[\overline{u_k u_l}\left(\overline{u_i u_j}\right)_{,l}\right] \tag{5}$$

$$\text{HL} : \quad -T_{ijk} = c_{s2}\frac{k}{\epsilon}\left[\overline{u_i u_l}\left(\overline{u_j u_k}\right)_{,l} + \overline{u_j u_l}\left(\overline{u_k u_i}\right)_{,l} + \overline{u_k u_l}\left(\overline{u_i u_j}\right)_{,l}\right] \tag{6}$$

$$\text{MH} : \quad -T_{ijk} = c_{s3}\frac{k^2}{\epsilon}\left[\left(\overline{u_i u_j}\right)_{,k} + \left(\overline{u_i u_k}\right)_{,j} + \left(\overline{u_j u_k}\right)_{,i}\right] \tag{7}$$

with c_{s1}=0.22, c_{s2}=0.11 and c_{s3}=2/3c_{s2}. These are essentially gradient diffusion models in which DH and HL have non-isotropic diffusion coefficients, but that for MH is isotropic. HL and MH diffusion models preserve symmetry in the indices but the DH model does not. In a general three-dimensional flow, the HL model requires the evaluation of 27 derivatives, whereas the DH and MH models each contain only 9 derivatives. For developed thin shear flow with $(\ )_{,1} = (\ )_{,3} = 0$, the diffusion terms are assembled in Table 1. These models result in expressions for the diffusion of k which are different from those usually given in two-equation models.

2.4 Pressure-Strain Models

Five models for the pressure-strain correlation are examined in this study. These are the quasi-isotropic version (model 1) of LRR, with and without wall-proximity treatment, the dynamical-systems based model of SSG, and the non-linear models of SL and FLT, both of which are derived from realizability constraints. The LRR model without wall treatment is denoted by LRRNW in this paper. In their model 1, LRR proposed to account for wall-proximity effects

by making coefficients in the equations functions of the average distance from walls. In the simpler version (model 2) usually called the Gibson-Launder model, they are treated as wall-reflection terms. It should be noted that these wall-reflection terms are not near-wall corrections in the conventional sense, since they are applicable to the fully turbulent region beyond the viscous sublayer and the buffer zone, and they still have significant contributions at the center of the channel. However, there is uncertainty as to how rapidly the functions should decay with distance from walls, or how to estimate average distance from walls in complex geometries. Hence, it is now generally accepted that the need for wall-proximity treatment is an undesirable feature in a pressure-strain model. The comparison between LRR and LRRNW serves merely to show the dominant role wall reflection terms may play in determining the anisotropy levels.

The primary question that we address in this study is how do the sophisticated Reynolds stress models perform in a 'building block' inhomogeneous shear flow such as channel flow. We are interested in evaluating the performance of these high Reynolds number models in a region (y+ > 200) *away* from the wall - an issue separate from near-wall turbulence modeling. Therefore, the same wall-function treatment is used to bridge the near-wall region in all the models considered here.

The pressure-strain models can be written in terms of the anisotropy tensor $b_{ij}(\equiv \overline{u_i u_j}/2k - \frac{1}{3}\delta_{ij})$, the rate of strain tensor $S_{ij}\left(\equiv \frac{\partial U_i}{\partial U_j} + \frac{\partial U_j}{\partial U_i}\right)$, the rotation tensor $W_{ij}\left(\equiv \frac{\partial U_i}{\partial U_j} - \frac{\partial U_j}{\partial U_i}\right)$, and the rate of production of turbulent kinetic energy P_k in the general form :

$$\begin{aligned}
\pi_{ij} \;=\; & \alpha_0\epsilon b_{ij} + \alpha_1\epsilon\left(b_{ik}b_{jk} - 1/3\mathrm{II}\delta_{ij}\right) + \alpha_2 k S_{ij} + \alpha_3 P_k b_{ij} + \\
& \underbrace{+k\{\alpha_4\left(b_{ik}S_{jk} + b_{jk}S_{ik} - 2/3\delta_{ij}b_{kl}S_{kl}\right) + \alpha_5\left(b_{ik}W_{jk} + b_{jk}W_{ik}\right)}_{linear\ terms} \\
& \underbrace{+\alpha_6\left(b_{ik}b_{lk}S_{jl} + b_{jk}b_{lk}S_{il} - 2b_{kj}b_{li}S_{kl}\right) + \alpha_7\left(b_{ik}b_{lk}W_{jl} + b_{jk}b_{lk}W_{il}\right)}_{quadratic\ terms} \\
& \underbrace{+\alpha_8\left[b_{nl}b_{ln}\left(b_{ik}W_{jk} + b_{jk}W_{ik}\right) + 3b_{mi}b_{nj}\left(b_{mk}W_{nk} + b_{nk}W_{mk}\right)\right]\}}_{cubic\ terms}
\end{aligned} \tag{8}$$

The model coefficients $\alpha_0 \ldots \alpha_8$ may be, in general, functions of the invariants of the anisotropy tensor. The corresponding relations for the five pressure-strain models are presented in Table 2.

In the table, f is a wall-proximity function which takes a value of unity in the fully turbulent region near a wall and zero in a flow free from walls. LRR proposed a linear decay for f, but Demuren and Rodi (1984) found the wall effect too strong near the center of the channel, hence they prefer the quadratic form used in this paper. $\mathrm{II}(= b_{lk}b_{kl})$ and $\mathrm{III}(= b_{lk}b_{km}b_{ml})$ are, respectively the second and third invariants of the Reynolds stress anisotropy tensor and R_T is the turbulent Reynolds number. The constants c_μ and κ take the standard values 0.09 and 0.42, respectively.

The first line in equation (8) contains a mixture of terms representing both "slow" and "rapid" contributions to the pressure-strain correlation. The first term is the usual Rotta term for the return to isotropy. All the models have this term, which has a constant coefficient in the LRRNW and SSG models, but is a function of the wall-proximity variable in the LRR model, and a function of the invariants in the SL and FLT models. In the latter, the particular forms are derived to ensure that the turbulence remains realizable in the two-component limit as the wall is approached. Such a condition is never approached in the present study since the integration is not performed all the way down to the wall. In the FLT model, unlike all the other models, this term does not contain the full return to isotropy term, since the value of the coefficient α_0 may become less than 2 when the second invariant II gets very small. The remaining contribution, which ensures the return to isotropy is contained in their approximation for $\epsilon_{ij}\left(= 2/3\delta_{ij}\epsilon + \left[2 - 2\mathbf{F}^{1/2}\right]b_{ij}\epsilon\right)$. The treatment corresponds more nearly to the usual practice if the second part of this expression is combined with the return to isotropy term. Only the SSG and FLT models have a non-linear contribution to the return to isotropy. The last two terms on the first line are contributions to the "rapid" part, the first of these is a linear term and the second is quadratic in b_{ij}, since P_k itself is linear in b_{ij}. The major contributions to the "rapid" part of the pressure-strain correlation are those collection of terms in lines 2 to 4 of equation (8). All models contain the linear terms.

Only the SL and FLT terms contain the quadratic terms and only the FLT model has terms which are cubic in the anisotropy stress tensor.

2.5 k-ϵ Model

Calculations were also made with the standard high-Reynolds number form of the k-ϵ turbulence model. The equations for k and ϵ can be expressed in tensor notation as:

$$\frac{\partial}{\partial x_l}(U_l k) = D_k + P_k - \epsilon \tag{9}$$

$$\frac{\partial}{\partial x_l}(U_l \epsilon) = D_\epsilon + c_{\epsilon_1}\frac{\epsilon}{k}P_k - c_{\epsilon_2}\frac{\epsilon^2}{k} \tag{10}$$

In the standard form of the model the terms D_k and D_ϵ are approximated by gradient diffusion relations as:

$$D_k = \frac{c_\mu}{\sigma_k}\left(\frac{k^2}{\epsilon}k_{,l}\right)_{,l} \tag{11}$$

$$D_\epsilon = \frac{c_\mu}{\sigma_\epsilon}\left(\frac{k^2}{\epsilon}\epsilon_{,l}\right)_{,l} \tag{12}$$

These equations are routinely solved, even when the interest is only in the solution with the second-moment closure models. ϵ is of course required for closure. The trace of the Reynolds stresses should be equal to 2k, so that the solution of the k-equation is redundant. It serves, in this study, solely as an additional check for the convergence and the consistency of the solution. Thus, it was required that half the trace of the computed Reynolds stress distributions should agree with the computed distributions of k to within 0.2%, at every point in the flow. For consistency in this case, D_k must take the forms given in Table 1. The emphasis in the present study is on the models for the pressure-strain correlation and the turbulent diffusion, so the use of anisotropy diffusion coefficients in the ϵ-equation, as proposed by HL may becloud the issue. The empirical constants in equations (9–12) are : σ_k = 1.0 ; σ_ϵ = 1.3 ; $c_{\epsilon 1}$ = 1.44 ; $c_{\epsilon 2}$ =1.92.

Note that some authors (for example SL) use versions of the k-ϵ equation with different values for the model coefficients. The question arises as to whether such differences change the equilibrium Reynolds stress anisotropies in the log-layer. Consider the Reynolds stress equation in the fully-developed, incompressible channel flow

$$D_{ij} + P_{ij} + \pi_{ij} - \frac{2}{3}\epsilon\delta_{ij} = 0 \tag{13}$$

In the log-layer, where diffusion can be neglected and (13) becomes

$$P_{ij} + \pi_{ij} - \frac{2}{3}\epsilon\delta_{ij} = 0$$

or

$$\frac{P_{ij}}{\epsilon} + \frac{\pi_{ij}}{\epsilon} - \frac{2}{3}\delta_{ij} = 0 \tag{14}$$

All the models for π_{ij} are of the form $\frac{\pi_{ij}}{\epsilon} = f\left(b_{ij}, \frac{Sk}{\epsilon}\right)$ in a simple shear flow. Since $P_k = \epsilon$ in the log-layer, we have $\frac{Sk}{\epsilon} = -\frac{1}{2b_{12}}$, and thus $\frac{\pi_{ij}}{\epsilon} = f(b_{ij})$. Similarly, $\frac{P_{ij}}{\epsilon} = g\left(b_{ij}, \frac{Sk}{\epsilon}\right) = g(b_{ij})$. Thus, equation (14) becomes an algebraic equation for b_{ij} *independent* of ϵ. Consequently, the anisotropy tensor b_{ij} in the log-layer is independent of the form and coefficients of the ϵ–equation. Note that b_{ij} is determined completely by the form of the pressure-strain model and should be constant if there is no explicit y dependence in the model.

2.6 Solution Procedure

The problem, as formulated, is strictly one-dimensional, but a two-dimensional TEACH-type code which solves the full, time-averaged, Navier-Stokes equations is utilized, in order to ease extension to other flow cases in future studies. The redundant terms are simply set to zero in the present study. The initial conditions for the mean flow and turbulent stresses are taken from the simulation data of Kim, Moin and Moser (1987), but these are scaled up to yield an effective Reynolds number (based on bulk mean velocity and half width) of 5.2×10^4, to coincide with the highest Reynolds number of Laufer's experiments. The computed results (normalized with U_τ) are similar to those obtained (Demuren and Sarkar, 1991) at a higher Reynolds number ($\sim$

4 x 10^5). Computations are performed for half of the channel from the lower wall to the mid-plane. The calculations use 32 grid points in the transverse direction and sufficient lengths (over 400 half-widths) in the longitudinal direction to ensure full flow development. Computations with twice as many points in each direction do not produce significantly different results. The objective of this work is to compare the behavior of various pressure-strain and diffusion models, so the computations are for the high Reynolds number flow region only in which the viscous sublayer is not resolved but is bridged using the standard wall-function method. Along the line of nodes nearest to the walls ($y^+ \sim 30$) local equilibrium is assumed: The streamwise velocity component is specified based on the logarithmic velocity of the wall ($U^+ = \frac{1}{\kappa} ln\ y^+ + 5.0$) ; $k = U_\tau^2 / c_\mu^{1/2}$; $\epsilon = U_\tau^3 / (\kappa y)$; $\overline{u_1^2} = 1.07\ k$; $\overline{u_2^2} = 0.41\ k$; $\overline{u_3^2} = 0.52\ k$; $\overline{u_1 u_2} = -0.30\ k$. The specification of the second set of boundary conditions is that the first derivative of all dependent variables is set to zero normal to the symmetry plane.

3. Results and Discussion

The results of the computations to test the turbulent diffusion models are compared to results obtained with the k-ϵ model and experimental data in Figs. 2–4. For each of the computations with the second-moment closure the pressure-strain correlations are modelled with the SSG form, but the three diffusion models given by equations (5–7) are used. Profiles of the streamwise velocity are presented in semi-logarithmic form in Fig. 2. All the profiles agree very well with the log-law ($U^+ = \frac{1}{\kappa} ln\ y^+ + 5.0$) in the inner layer. The results with the k-ϵ model display a pronounced wake region, but the second-moment closures give only a small wake region. Since the channel flow has a favorable pressure gradient, the wake region is of course much smaller than that for a flat plate boundary layer. Measurements by Clark (1968), Laufer (1951) and Hussain and Reynolds (1975) also show a very small wake region. Hence, the velocity profiles are well predicted by all the diffusion models. Another test of the diffusion models is in the prediction of the Reynolds stress anisotropy tensor in the relaxation region $0.7 > y/\delta < 1.0$. Figure 3 compares these results with the data of Laufer for the 4 non-zero components. As seen in the

11 and 22 components, the MH model produces the strongest rate of relaxation towards isotropy as the center of the channel is approached, and it gives the best agreement with experimental data. The DH model shows little change in the anisotropy level between the log-layer and the center of the channel. The results for the HL model lie somewhat between the other two. For the 33 component, the DH model shows slightly better agreement with the data. These results can be explained by considering order of magnitude estimates of the diffusion terms given in Table 1. DH and HL models have coefficients c_{s1} and c_{s2} which are respectively 3 and 1.5 times larger than that for the MH model. But they are modified by anisotropy coefficients, the most significant of which is $\overline{u_2^2}/k$, with a value 0.4 in the log-layer. Order of magnitude estimates then show that the diffusion terms for $\overline{u_1^2}$ are roughly equal, but for $\overline{u_2^2}$, the MH model yields a diffusion term which is about 2.5 times greater than that for the DH model and 1.7 times greater than that for the HL model. The budget of the Reynolds stresses from the present study (not shown) and from the DNS data of Kim (unpublished), shows that the diffusion of the normal stresses are positive in the central part of the channel ($y/\delta > 0.5$) while the diffusion of the shear stress is negative. Thus, an increase in the diffusion of $\overline{u_2^2}$ would increase $\overline{u_2^2}$ and move b_{22} closer to zero, thereby reducing the anisotropy, if $\overline{u_1^2}$ and $\overline{u_3^2}$ are not correspondingly increased. This is the case here, since the diffusion models yield magnitudes which are more nearly equal for $\overline{u_1^2}$ and $\overline{u_3^2}$. Therefore, the MH model which has the largest diffusion term for $\overline{u_2^2}$ produces the fastest rate of relaxation towards isotropy and the best agreement with experimental data. Similar order of magnitude estimates can be used to explain the results for b_{33} and b_{12}. Since the diffusion of $\overline{u_1 u_2}$ is negative, a higher magnitude will produce a lower value of b_{12}. The comparisons of the predicted turbulent kinetic energy are presented in Fig. 4. The predictions are in reasonably good agreement with the data. The slight differences between the predicted results can also be explained by the aforementioned order of magnitude estimates.

The predictions with the five pressure-strain models are compared in Figs. 5–7. The MH model for the turbulent diffusion is used in each case. Figure 5 shows that all models except the SL model give reasonable prediction of the mean streamwise velocity profile in agreement

with the universal logarithmic law of the wall. The explanation for this can be found in Fig. 6 and Table 3. The main requirement for the correct prediction of the mean velocity is that the model should yield an accurate distribution of the shear stress. The latter is related to the b_{12} component of the Reynolds stress anisotropy tensor. Table 3 shows that this component is reproduced fairly accurately by all but the SL model. In the inner core of the flow ($y/\delta < 0.8$) the SL model underpredicts b_{12} by about 30%. Now, in the equilibrium layer for thin shear flows the ratio of production to dissipation is given by :

$$\frac{P_k}{\epsilon} = -2\, b_{12}\left(\frac{Sk}{\epsilon}\right) \tag{15}$$

and since P_k/ϵ is approximately unity the normalized shear rate (Sk/ϵ) is inversely proportional to b_{12}. Underprediction of b_{12} will produce excessive shear rate and hence a poor velocity profile. Experimental and DNS data suggest that Sk/ϵ should be equal to about 3.3 in the inner layer. Most of the models predict values in the range 3.0 — 3.5, but the SL model predicts values of around 4.3. The latter is not surprising since Speziale and Mac Giolla Mhuiris (1989) had reported that the SL model predicts equilibrium values, in homogeneous shear flow, of b_{12} and Sk/ϵ of –0.12 and 6.93, which are respectively, lower and higher in magnitudes than experimental values by about 20%. The channel flow is of course not a homogeneous shear flow but there are some similarities. For example b_{ij} and Sk/ϵ have constant values in both the log-layer of the channel and the equilibrium homogeneous shear flow.

The comparisons of the normal components of the Reynolds stress anisotropy tensor in Fig. 6 are even more instructive. A comparison of results obtained with the LRR model to those with the LRRNW model shows the effects of the wall-reflection terms. They produce a significant increase in the anisotropy of 11 and 22 components, with little effect on the 33 component. Although the increase in anisotropy is strongest near the wall, it remains pronounced even at the center of the channel. This is contrary to expectation. The dilemma is how to devise a function for the wall reflection effects which decays at the right rate away from the wall that would also be general enough for application to more complex flows. Better still, the model should not require wall reflection terms.

If we consider the level of anisotropy in the inner layer, the SSG model (dash-dot curves in Fig. 6) gives the closest predictions of b_{11}, b_{22} and b_{33}. The LRR model gives reasonable predictions for b_{11} and b_{22}, but not for b_{33}. Both these models are relatively simple, without the quadratic and cubic terms in equation (8). Their good performance is probably due to their superior calibration for homogeneous flows. The SSG model was calibrated in a dynamical systems approach using data from the nearly-homogeneous shear flow experiments of Tavoularis and Corrsin (1981). The LRR model was calibrated with the earlier (and probably less reliable) experimental data for nearly-homogeneous shear flow of Champagne, Harris and Corrsin (1970) and the wall-reflection part of the model used a consensus of near-wall data. It is surprising that the FLT model which contains both the quadratic and cubic terms in equation (8) does not give predictions which are superior to the much simpler models. Furthermore, b_{33} shows an increase in anisotropy towards the center of the channel. Perhaps the calibration of the model is to blame. Numerical experiments indicate that the level of anisotropy in the 11 and 22 components can be increased by increasing the magnitude of the coefficient of the cubic terms, α_8 in equation (8). However, this produces little effect on the 33 component. Again the predictions by the SL model of b_{11} and b_{22} in the channel flow are much lower than in the experiments. Correspondingly, b_{33} is much too high. Such underprediction of b_{11} and b_{22} has also been observed in homogeneous shear flow (Speziale and Mac Giolla Mhuiris, 1989). The values of the Reynolds stress anisotropy tensor in the log-layer are summarized for all models and the experimental data in Table 3.

A notable feature of the predictions is that the models do not fully reproduce the rapid relaxation towards isotropy (especially in b_{11} and b_{33}) in the outer-layer ($y/\delta > 0.75$) in response to the relaxation in the shear rate. Figure 8 shows a comparison of the profiles of Sk/ϵ obtained from the DNS results of Kim (unpublished), and predictions with the k-ϵ model and the SSG Reynolds stress closure model. These all show that Sk/ϵ is nearly constant in the inner layer and starts to decay rapidly beyond $y/\delta = 0.7$. All the models show only a mild decay in the anisotropy level of the 11 and 33 components in this region, but DNS and experimental data presented in

Fig. 9 all show strong relaxation towards isotropy in correspondence with the decay of the shear rate. The main effects of increasing the Reynolds number are seen to be the reduction of the anisotropy close to the wall and a faster rate of return to isotropy near the center of the channel. Figure 7 shows that all the pressure-strain models (in conjunction with the MH diffusion model) produce reasonably good prediction of the turbulent kinetic energy.

4. Concluding Remarks

The k-ϵ model and the second-moment closure models, apart from the SL model, produce similar predictions of the mean flow velocity, which agree well with the logarithmic law of the wall over most of the channel cross-section. In agreement with experimental observations in channel flows, there is only a small wake component. The SL model underpredicts the shear stress, and this leads to poor prediction of the mean flow velocity. All the other models predict the shear stress distribution correctly.

The different models for the turbulent diffusion have little effect on the normal components of the Reynolds stress tensor in the log-layer, but strongly influence the rate of relaxation towards isotropy in the outer layer near the center of the channel. The MH diffusion model gives the best agreement with experimental data.

LRR and SSG pressure-strain models give the best prediction of the streamwise and transverse components of the Reynolds stresses. The LRR model requires wall-reflection terms to achieve this but the SSG model does not. The wall reflection terms remain pronounced in the outer layer. Such an outer-layer influence is perhaps physically inappropriate. Only the SSG model could predict the lateral component of the Reynolds stress anisotropy correctly.

The models failed to predict correctly the rate of relaxation of the streamwise and lateral components of the Reynolds stresses towards isotropy when the shear rate decreases in the outer layer $y/\delta > 0.7$.

The pressure strain models which performed well in the present study, such as the LRR and SSG models, are expected to give reasonable results in other equilibrium shear flows. But there is no indication as to their performance in other complex flows. That is a subject for future studies.

Acknowledgment

This work had its origin in the 1991 ICASE/LaRC Workshop on Turbulence and Transition. The computations were performed on the Cray YMP computer of the NAS program at NASA Ames Research Center, Moffet Field, California.

References

Amano, R.S. and Goel, P., 1987 "Investigation of Third-Order Closure Model for the Computation of Incompressible Flows in in a Channel with a Backward-Facing Step," ASME, J. Fluids Eng., Vol. 109, pp. 424–428.

Champagne, F.H., Harris, V.G., and Corrsin, S., 1970 "Experiments in nearly Homogeneous Turbulent Shear Flow," J. Fluid Mech., Vol. 41, pp. 81–139.

Clark, J. A., 1968 "A Study of Incompressible Turbulent Boundary Layers in Channel Flow," ASME J. Basic Eng., Vol. 90, pp. 455–467.

Comte-Bellot, G., 1965 "Ecoulement Turbulent Entre Deux Parois Paralleles," Publications Scientifiues et Techniques, du Ministere de L' air, No. 419.

Daly, B.J. and Harlow, F.H., 1970 "Transport Equations of Turbulence," Phys. Fluids, Vol. B, pp. 2634–2649

Demuren, A.O., 1992 "Multigrid Acceleration and Turbulence Models for Computations of 3D Turbulent Jets in Crossflow," Int. J. Heat Mass Trans., (in press).

Demuren, A.O., and Rodi, W., 1984 "Calculation of Turbulence-Driven Secondary Motion in Non-circular Ducts," J. Fluid Mech., Vol. 140, pp. 189–222.

Demuren, A.O., and Sarkar, S., 1992 "Application of Second-Moment Closure Models to Complex Flows: Part 1 – Wall Bounded Flows," Proc., ICASE/Langley Workshop on Turbulence and Transition, (in press).

Fu, S., Launder, B. E. and Tselepidakis, D. P., 1987 "Accomodating the Effects of High Strain Rates in Modelling the pressure-strain correlation," Dept. of Mech. Eng., UMIST Rept. TFD/87/5.

Hanjalic, K., and Launder, B.E., 1972 "A Reynolds Stress Model of Turbulence and its Application to Thin Shear Flows," J. Fluid Mech., Vol. 52, pp. 609–638

Hussain, A.K.M.F., and Reynolds, W.C., 1975 "Measurements in Fully Developed Turbulent Channel Flow," ASME J. Fluids Eng., Vol. 97, pp. 568–578

Kim, J., Moin, P. and Moser, R., 1987 "Turbulence Statistics in Fully Developed Channel Flow at low Reynolds Number," J. Fluid Mech., Vol. 177, pp. 133–166.

Klein, A., 1981 "Review: Turbulent Developing Pipe Flow," Trans. ASME, J. Fluids Eng., Vol. 103, pp. 423–429.

Laufer, J., 1951 "Investigation of Turbulent Flow in a Two-Dimensional Channel," NACA Report 1053.

Launder, B.E., Reece, G.J., and Rodi, W., 1975 "Progress in the Development of a Reynolds Stress Turbulence Closure," J. Fluid Mech., Vol. 68, pp. 537–566.

Mellor, G.L., and Herring, H.J., 1973 "A Survey of Mean Turbulent Field Closure," AIAA J., Vol. 11, pp. 590–599.

Rotta, J.C., 1951 "Statistische Theorie nichthomogener Turbulenz," Z. Phys. Vol. 129, pp. 547–572.

Shih, T.-H., and Lumley, J.L., 1985 "Modeling of Pressure Correlation Terms in Reynolds Stress and Scalar Flux Equations, Tech. Rep. FDA-853, Cornell University.

Speziale, C.G. 1991 "Analytical Methods for the Development of Reynolds-Stress Closures in Turbulence," Ann. Rev. Fluid Mech., Vol. 23, pp. 107–157.

Speziale, C.G., and Mac Giolla Mhuiris, N., 1989 "On the Prediction of Equilibrium States in Homogeneous Turbulence", J. Fluid Mech., Vol. 209, pp. 591–615.

Speziale, C.G., Sarkar, S. and Gatski, T.B., 1991 "Modelling the Pressure-Strain Correlation of Turbulence: An Invariant Dynamical Systems Approach," J. Fluid Mech., Vol. 227, pp. 245–272.

Sykes, R.I., Lewellen, W.S. and Parker, S.F., 1986 "On the Vorticity Dynamics of a Turbulent Jet in Crossflow, J. Fluid Mech., Vol. 168, pp. 393–413.

Tavoularis, S. and Corrsin, S., 1981 "Experiments in nearly Homogeneous Turbulent Shear Flows with a uniform mean Temperature gradient," J. Fluid Mech., Vol. 104, pp. 311–347.

Table 1 Diffusion terms D_{ij} for developed thin shear flow

	DH	HL	MH
$\overline{u_1^2}$	$c_{s1}\left[\frac{k}{\epsilon}\left(\overline{u_2^2}\right)\left(\overline{u_1^2}\right)_{,2}\right]_{,2}$	$c_{s2}\left[\frac{k}{\epsilon}\left\{2(\overline{u_1u_2})(\overline{u_1u_2})_{,2} + \left(\overline{u_2^2}\right)\left(\overline{u_1^2}\right)_{,2}\right\}\right]_{,2}$	$c_{s3}\left[\frac{k^2}{\epsilon}\left(\overline{u_1^2}\right)_{,2}\right]_{,2}$
$\overline{u_2^2}$	$c_{s1}\left[\frac{k}{\epsilon}\left(\overline{u_2^2}\right)\left(\overline{u_2^2}\right)_{,2}\right]_{,2}$	$3c_{s2}\left[\frac{k}{\epsilon}\left(\overline{u_2^2}\right)\left(\overline{u_2^2}\right)_{,2}\right]_{,2}$	$3c_{s3}\left[\frac{k^2}{\epsilon}\left(\overline{u_2^2}\right)_{,2}\right]_{,2}$
$\overline{u_3^2}$	$c_{s1}\left[\frac{k}{\epsilon}\left(\overline{u_2^2}\right)\left(\overline{u_3^2}\right)_{,2}\right]_{,2}$	$c_{s2}\left[\frac{k}{\epsilon}\left(\overline{u_2^2}\right)\left(\overline{u_3^2}\right)_{,2}\right]_{,2}$	$c_{s3}\left[\frac{k^2}{\epsilon}\left(\overline{u_3^2}\right)_{,2}\right]_{,2}$
$\overline{u_1u_2}$	$c_{s1}\left[\frac{k}{\epsilon}\left(\overline{u_2^2}\right)(\overline{u_1u_2})_{,2}\right]_{,2}$	$c_{s2}\left[\frac{k}{\epsilon}\left\{2(\overline{u_1u_2})\left(\overline{u_2^2}\right)_{,2} + \left(\overline{u_2^2}\right)(\overline{u_1u_2})_{,2}\right\}\right]_{,2}$	$2c_{s3}\left[\frac{k^2}{\epsilon}(\overline{u_1u_2})_{,2}\right]_{,2}$
k	$c_{s1}\left[\frac{k}{\epsilon}\left(\overline{u_2^2}\right)(k)_{,2}\right]_{,2}$	$c_{s2}\left[\frac{k}{\epsilon}\left\{\left(\overline{u_2^2}\right)(k)_{,2} + \left(\overline{u_2^2}\right)\left(\overline{u_2^2}\right)_{,2} + (\overline{u_1u_2})(\overline{u_1u_2})_{,2}\right\}\right]_{,2}$	$c_{s3}\left[\frac{k^2}{\epsilon}\left\{(k)_{,2} + \left(\overline{u_2^2}\right)_{,2}\right\}\right]_{,2}$

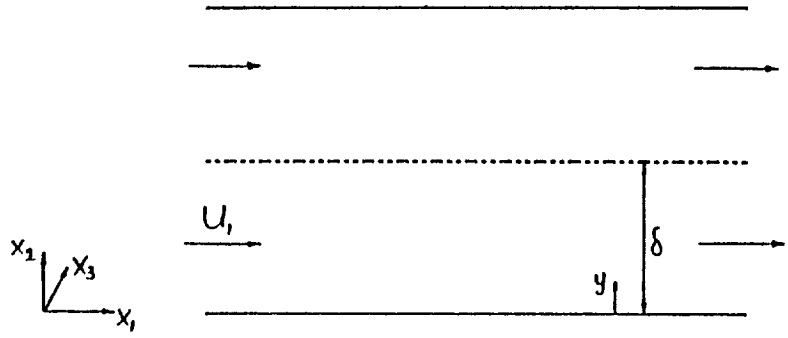

Figure 1 Geometry and coordinate system for plane channel flow.

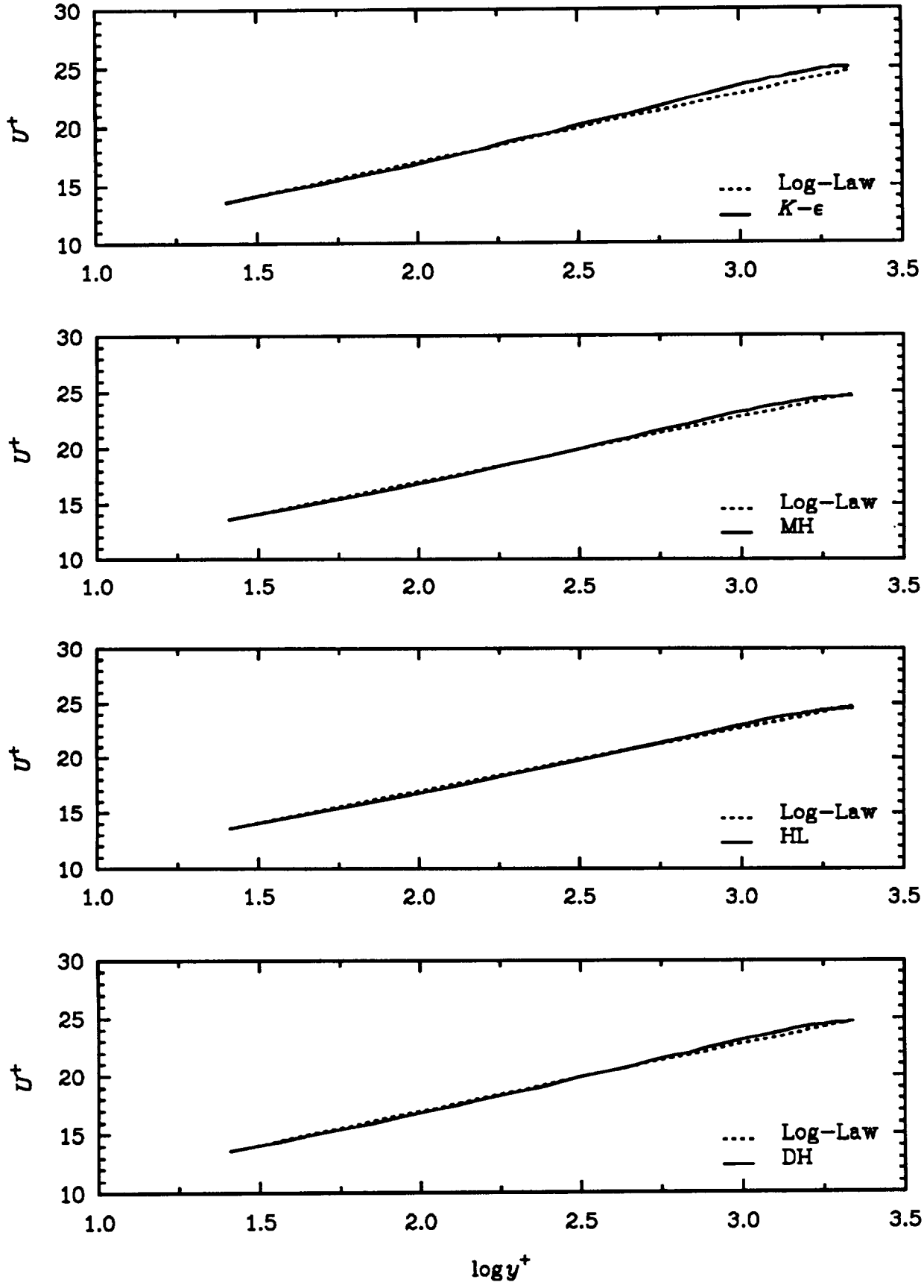

Figure 2 Comparison of velocity profiles computed with the SSG pressure–strain model and various diffusion models to the log–law.

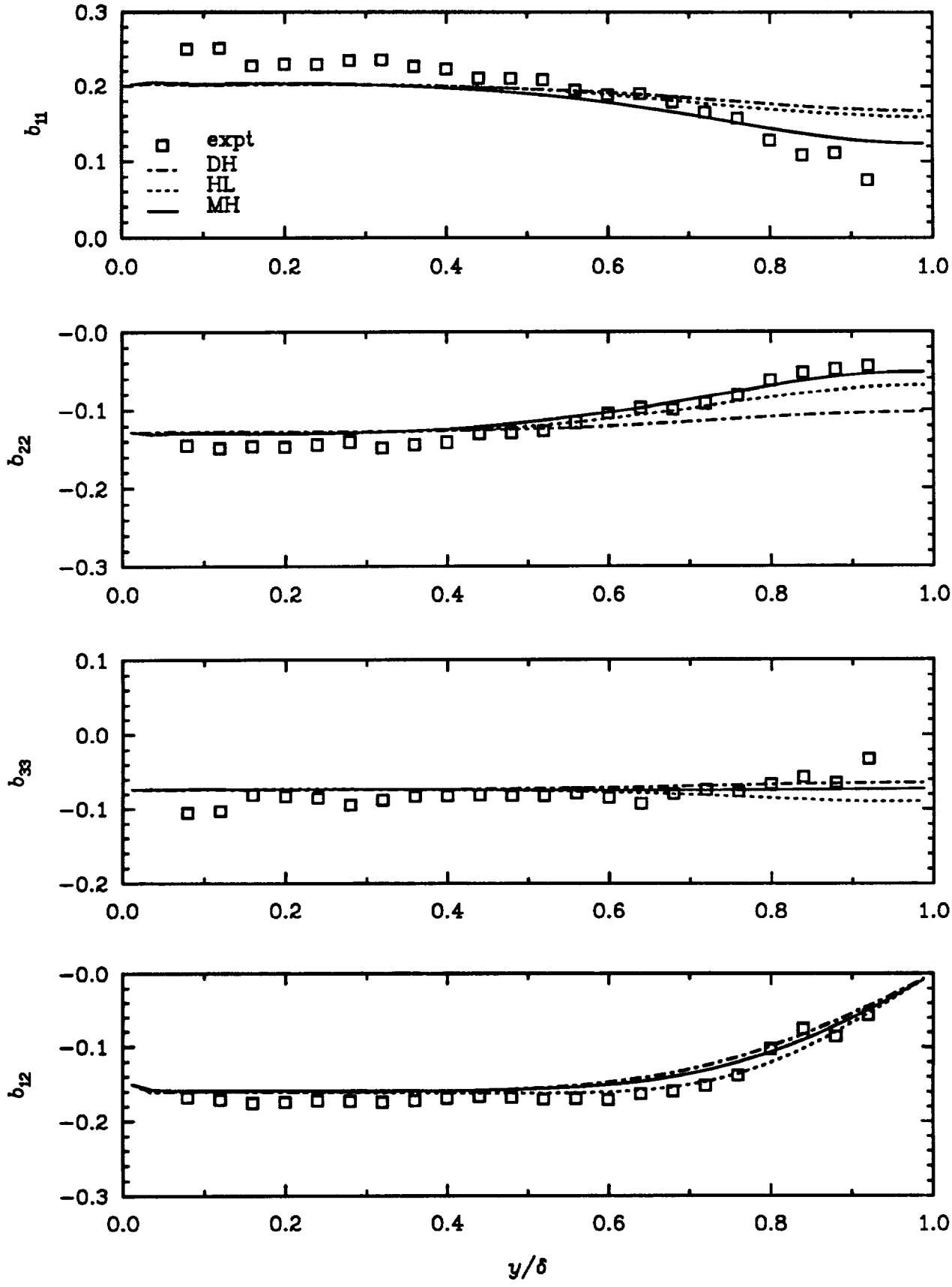

Figure 3 Comparison of components of the Reynolds stress anisotropy tensor computed with the SSG pressure–strain model and three diffusion models to experimental data of Laufer (1951).

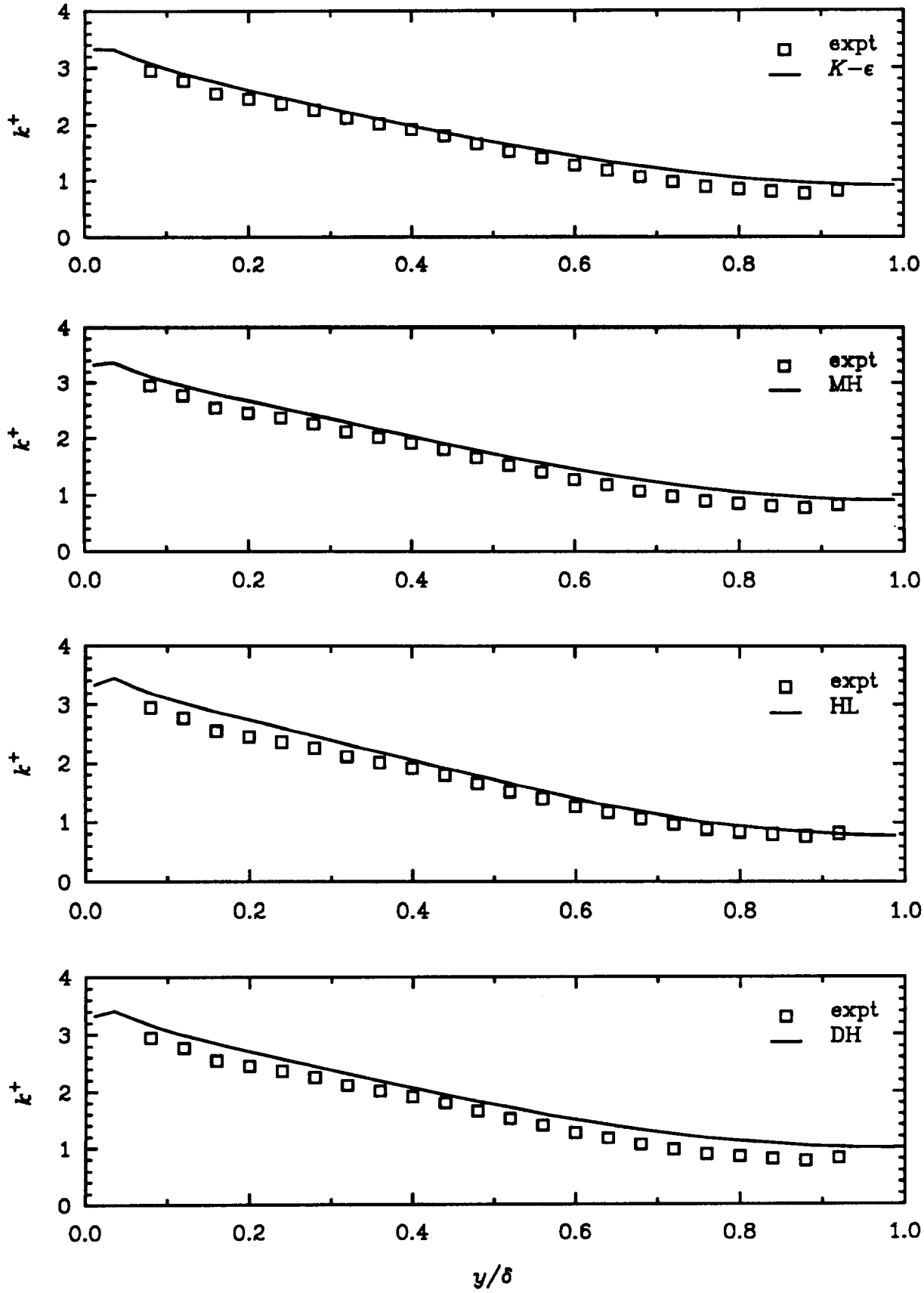

Figure 4 Comparison of profiles of the turbulent energy computed with the SSG pressure–strain model and various diffusion models to experimental data of Laufer (1951).

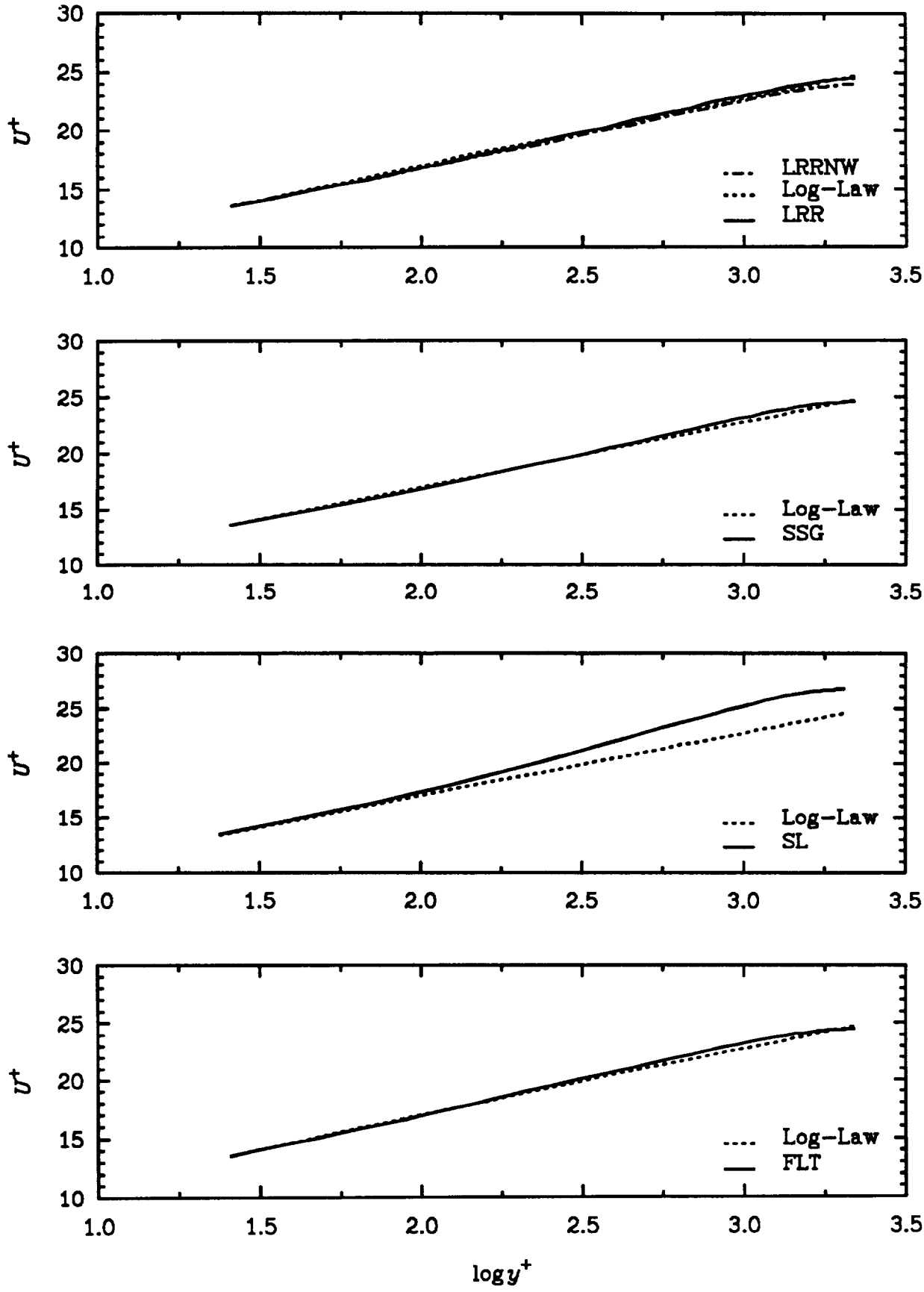

Figure 5 Comparison of velocity profiles computed with the MH diffusion model and various pressure–strain models to the log–law.

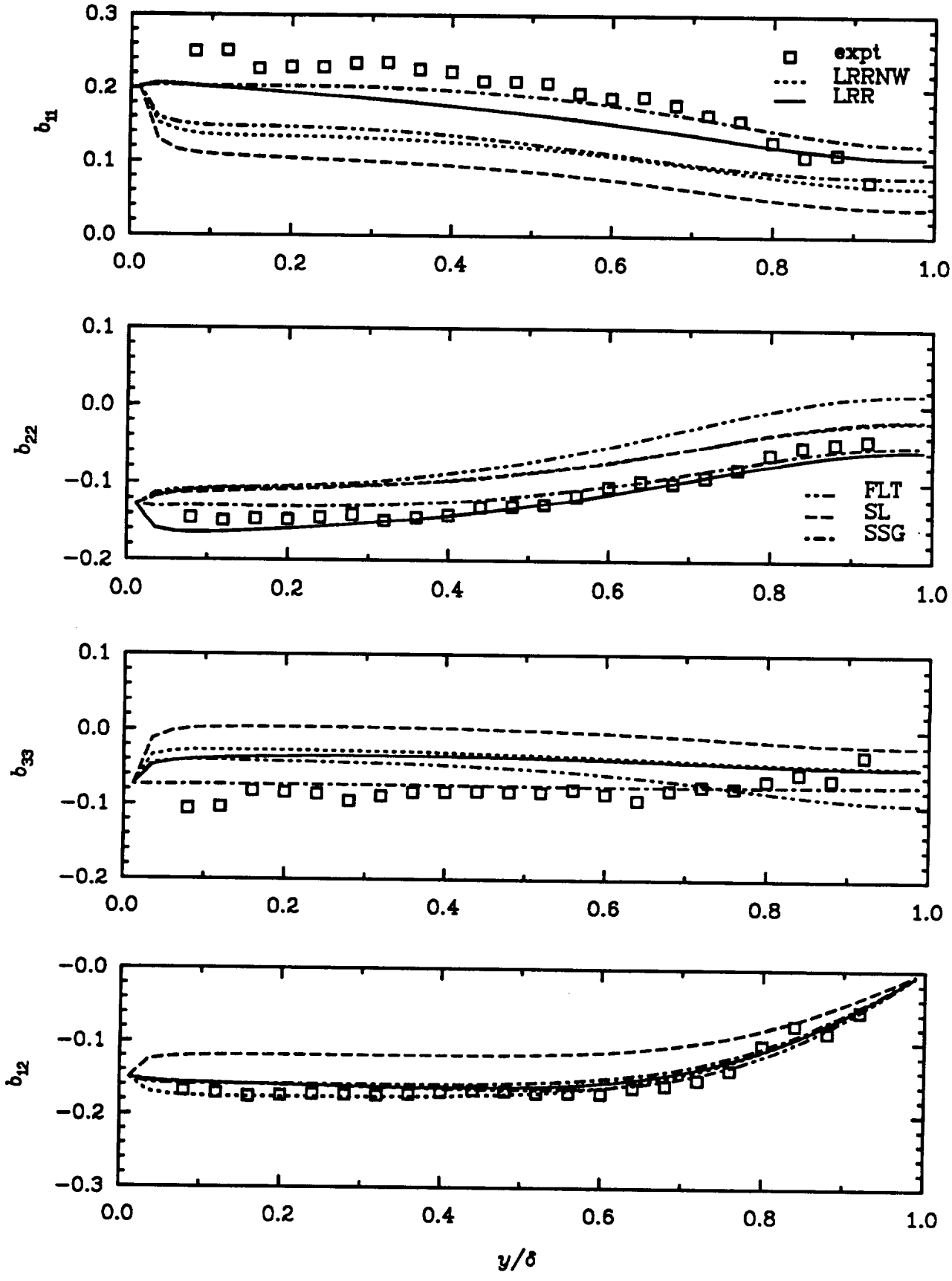

Figure 6 Comparison of components of the Reynolds stress anisotropy tensor computed with the MH diffusion model and various pressure–strain models to experimental data of Laufer (1951).

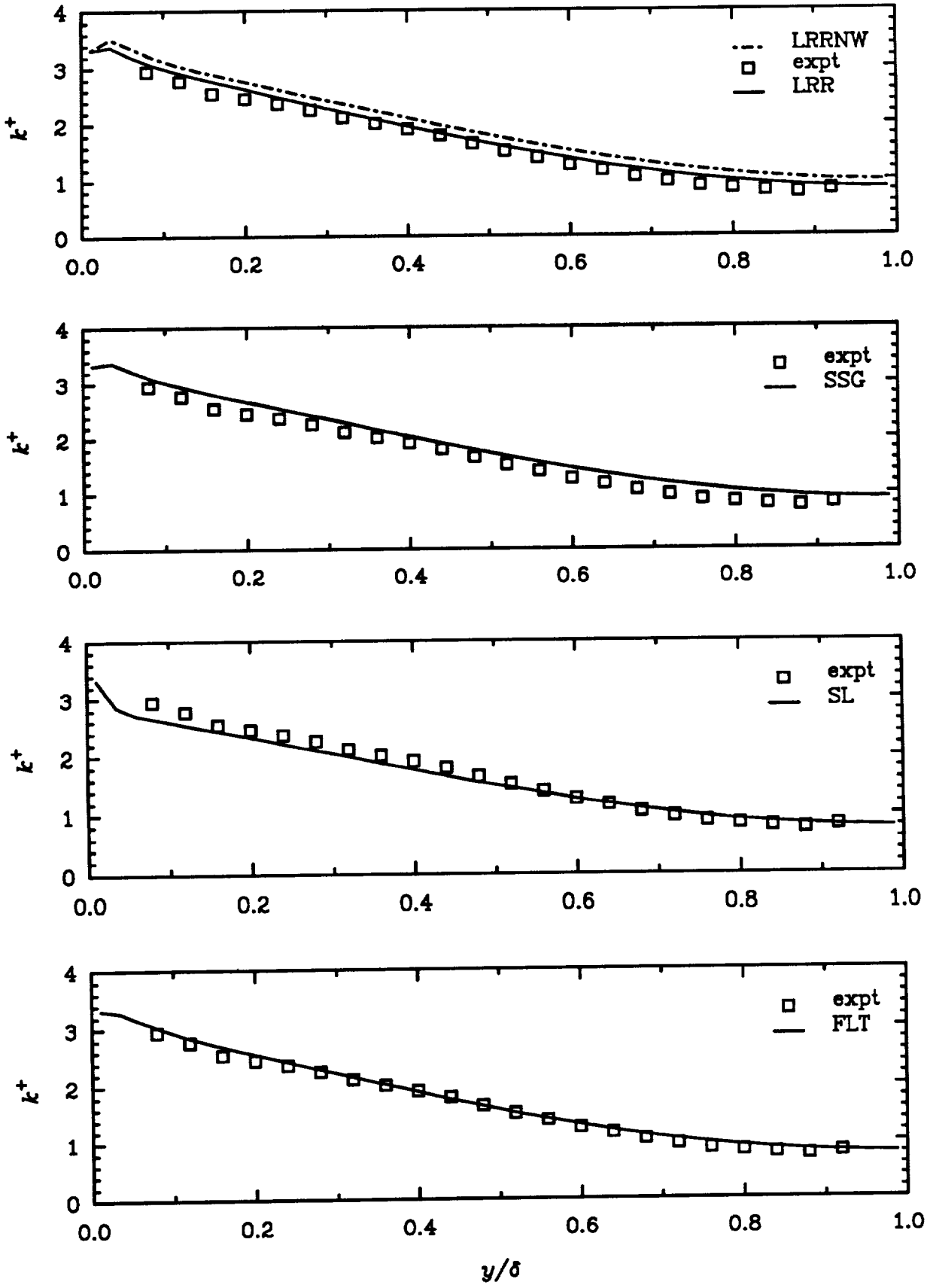

Figure 7 Comparison of profiles of the turbulent energy computed with the MH diffusion model and various pressure–strain models to experimental data of Laufer (1951).

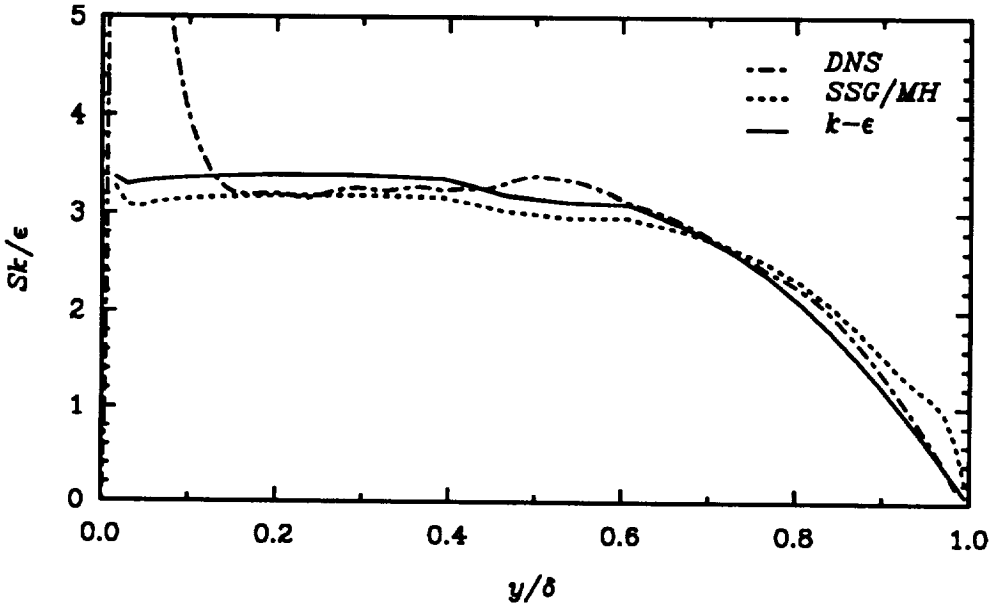

Figure 8 Comparison of computed shear rate (Sk/ϵ) in channel flow.

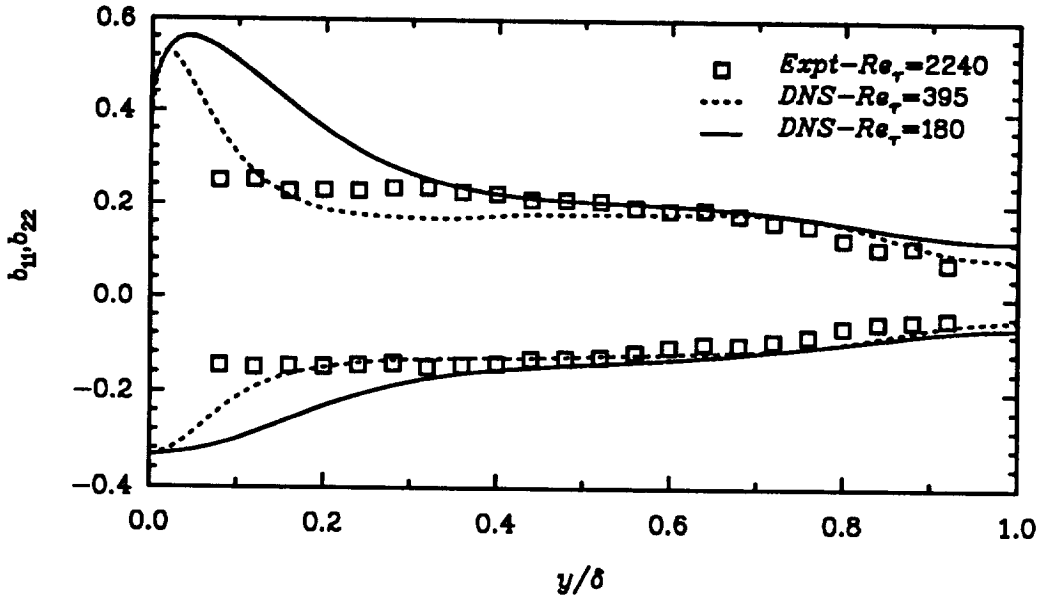

Figure 9 Comparison of Reynolds stress anisotropy tensor in channel flow from DNS of KMM (1987) and Kim (unpublished) and experiments of Laufer (1951

REPORT DOCUMENTATION PAGE

Form Approved
OMB No. 0704-0188

1. AGENCY USE ONLY (Leave blank)	2. REPORT DATE	3. REPORT TYPE AND DATES COVERED
	April 1992	Contractor Report

4. TITLE AND SUBTITLE
SYSTEMATIC STUDY OF REYNOLDS STRESS CLOSURE MODELS IN THE COMPUTATIONS OF PLANE CHANNEL FLOWS

5. FUNDING NUMBERS
C NAS1-18605
WU 505-90-52-01

6. AUTHOR(S)
A. O. Demuren
S. Sarkar

7. PERFORMING ORGANIZATION NAME(S) AND ADDRESS(ES)
Institute for Computer Applications in Science and Engineering
Mail Stop 132C, NASA Langley Research Center
Hampton, VA 23665-5225

8. PERFORMING ORGANIZATION REPORT NUMBER
ICASE Report No. 92-19

9. SPONSORING/MONITORING AGENCY NAME(S) AND ADDRESS(ES)
National Aeronautics and Space Adminstration
Langley Research Center
Hampton, VA 23665-5225

10. SPONSORING/MONITORING AGENCY REPORT NUMBER
NASA CR-189646
ICASE Report No. 92-19

11. SUPPLEMENTARY NOTES
Langley Technical Monitor: Michael F. Card
Final Report

Submitted to ASME Journal of Fluids Engineering

12a. DISTRIBUTION/AVAILABILITY STATEMENT
Unclassified - Unlimited

Subject Category 34

12b. DISTRIBUTION CODE

13. ABSTRACT *(Maximum 200 words)*

This paper investigates the roles of pressure-strain and turbulent diffusion models in the numerical calculation of turbulent plane channel flows with second-moment closure models. Three turbulent diffusion and five pressure-strain models are utilized in the computations. The main characteristics of the mean flow and the turbulent fields are compared against experimental data. All the features of the mean flow are correctly predicted by all but one of the Reynolds stress closure models. The Reynolds stress anisotropies in the log layer are predicted to varying degrees of accuracy (good to fair) by the models. None of the models could predict correctly the extent of relaxation towards isotropy in the wake region near the center of the channel. Results from the direct numerical simulation are used to further clarify this behaviour of the models.

14. SUBJECT TERMS	15. NUMBER OF PAGES
turbulence modeling	29
	16. PRICE CODE: A03

17. SECURITY CLASSIFICATION OF REPORT	18. SECURITY CLASSIFICATION OF THIS PAGE	19. SECURITY CLASSIFICATION OF ABSTRACT	20. LIMITATION OF ABSTRACT
Unclassified	Unclassified		

NSN 7540-01-280-5500

Standard Form 298 (Rev 2-89)
Prescribed by ANSI Std Z39-18
298-102

NASA-Langley, 1992